Annals of Nuclear Cardiology Vol. 8 No. 1 103–108

TECHNICAL POINT OF VIEW

Construction of a Phantom for Image Quality Evaluation in PET/MRI System

Yasuyuki Takahashi, PhD[1)], Ayaka Nemoto, MS[2)], Shota Hosokawa, PhD[1)], Hiroshi Ito, MD, PhD[2), 3)] and Noboru Oriuchi, MD, PhD[2), 4)]

Received: November 24, 2021/Revised manuscript received: April 22, 2022/Accepted: May 19, 2022
J-STAGE advance published: August 5, 2022

Abstract

***Background*: There is no phantom for image quality test in magnetic resonance imaging combined with positron emission tomography systems (PET/MRI systems). In MRI, radioactive water phantom containing 2-deoxy-2-[F-18] fluoro-D-glucose (^{18}F-FDG) cannot be used due to the dielectric effect. Even for phantoms filled with MR-available solutions, the source current of the RF coil is strongly disturbed as the diameter of the phantom increases. Stable MR images require proper phantom size and solution selection. Previous reports have not provided these details. Other than that, few existing phantoms evaluate negative signals such as N-13 ammonia (^{13}N-NH_3). We created a phantom for PET/MRI system for image quality test.**

***Methods*: The phantom for the PET/MRI system was assembled in two portions. One portion is a signal part containing ^{18}F-FDG radioactive water. The other portion is filled with polyvinyl alcohol glue to construct MRI image to generate μ-map. The glue part is allowed to rewrite the table position overlaps with the first layer, and attenuation correction is performed. Signals are set as positive (4 times and twice higher than background radioactivity) and negative (no radioactivity) columns with different sizes (15 mm ϕ and 7 mm ϕ). The PET images with X-ray computed tomography-based attenuation correction (CT-AC) and MRI-AC were evaluated by %-contrasts, variation and uniformity.**

***Results*: The %-contrasts of the positive shallow signals with PET/magnetic resonance (MR) and PET/CT were 41.8% and 45.4%, respectively. And it of the positive deep signals with PET/MR and PET/CT were 40.7% and 44.9%. On the other hand, the %-contrasts of the negative shallow signals with PET/MR and PET/CT were 62.3% and 65.6%, respectively. And it of the negative deep signals with PET/MR and PET/CT were 60.7% and 63.7%. Moreover, the% Nj index of uniformity was 2.0% on PET/MRI images and 0.34% on PET/CT images. For negative signals that assume a decrease in myocardial blood flow, The image quality of MR-AC was almost the same as that of CT-AC. Consistency between the images after CT-AC and MR-AC correction were confirmed, and in particular, a stable MR-AC μ-map was obtained in the phantom study.**

***Conclusion*: The suggested prototype phantom for generating μ-map is reasonable and useful for evaluating PET/MRI image quality, based on the present standard.**

Keywords: MR-AC, PET/MRI system, Phantom, Polyvinyl alcohol glue
Ann Nucl Cardiol 2022; 8 (1): 103–108

Hybrid scanner of positron emission tomography (PET) and magnetic resonance imaging (MRI) (PET/MRI) is a useful imaging modality for the simultaneous assessment of pathophysiological information, such as metabolism, perfusion and anatomical information both spatially and temporally (1). Conventional imaging was used to be done with PET and MRI based on separate scanners (2). PET/X-ray computed tomography (CT) scanner does not perform acquisition of PET

doi: 10.17996/anc.22-00152

1) Department of Radiation Science, Hirosaki University Graduate School of Health Sciences, Hirosaki, Japan
2) Department of Advanced Clinical Research Center, Fukushima Medical University, Fukushima, Japan
3) Department of Radiology, Fukushima Medical University, Fukushima, Japan
4) Department of Nuclear Medicine, Fukushima Medical University, Fukushima, Japan

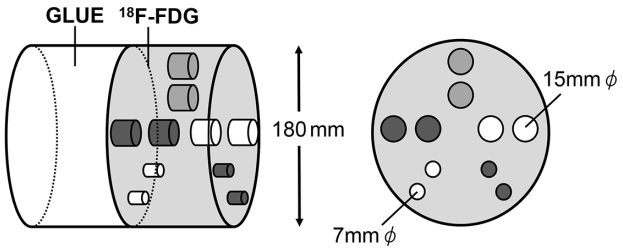

Figure 1 Configuration and layout of hot and cold columns in the phantom for performance evaluation of PET/MRI system.

The phantom consists of a glue part in the left half and a signal part in the right half, which contains 15 mm ϕ and 7 mm ϕ hot columns (dark columns: 4 times higher than BG radioactivity, light dark columns: twice higher than BG radioactivity) for positive signal and cold columns (no radioactivity) for negative signal placed at the shallow layer (20 mm from the surface) and the deep layer (60 mm from the surface).

and CT simultaneously as well. Myocardial PET study for the assessment of perfusion with ^{13}N-NH$_3$ (3–6), glucose metabolism with 2-deoxy-2- [F-18] fluoro-D-glucose (^{18}F-FDG) (7, 8), and more recently cardiac MRI with late gadolinium enhancement (LGE) (9, 10) has been used to diagnose myocardial viability. Therefore, PET/MRI is presently the most relevant tool to evaluate various pathophysiology, such as myocardial viability (11).

One of the fundamental limitation of PET/MRI is an inaccuracy of quantitation due to MR attenuation correction (MR-AC). In order to evaluate precision of PET/MRI including accuracy of MR-AC, phantom study is important. However, no fundamental phantom study has been conducted to verify PET/MRI performance, such as lesion detectability and quantitative assessment of hypoperfusion, i.e., negative signals.

In case of PET/CT, positron emitting radionuclides, such as ^{18}F is usually provided for the use of water-filled phantom (12). However, a human-sized water phantom cannot be used for PET/MRI due to the dielectric effect (13) for 3T MRI scanners. In this study, we constructed a prototype phantom that can be correctly used for a PET/MRI system and evaluated the detectability of both positive and negative signals.

Methods

Performance test phantom

A cylindrical phantom was developed for the performance test of PET/MRI. Dimension of the phantom is 180 mm in diameter and 300 mm in length (Figure 1). The diameter matched the size of a commercially available MRI performance test phantom. The phantom consist of two portions, i.e. signal part and glue part; a half portion for signal detection was filled with ^{18}F-FDG radioactive water of 5.3 kBq/ml as background (BG) and two concentrations of hot (4 times and twice higher than BG radioactivity) and cold (no radioactivity) columns of 15 mm ϕ and 7 mm ϕ placed at shallow and deep layers (20 mm and 60 mm depth from the surface, respectively) of the phantom, and the other half portion was uniformly filled with polyvinyl alcohol glue (Daiso-Sangyo, Hiroshima, Japan).

PET/MRI system

Data acquisition was done using a PET/MRI system (Biograph mMR, Siemens Healthcare GmbH, Erlangen, Germany) with software versions Syngo MR E11. PET acquisition was done for 10 minutes in a list mode with a matrix size of 172×172 (voxel size 4.2×4.2×4.2). PET images were reconstructed using the ordered subsets expectation maximization method (OS-EM; iteration times: 3, number of subsets: 21), and the Gaussian filter (4 mm) for post-processing. The μ-map was created by data acquisition of the glue part of the phantom. Attenuation correction was performed with the bed position changed from the glue part to the signal part. For MRI imaging, a field of view of 328 mm×500 mm (phase×read) with 2.6 mm×2.6 mm×3.1 mm voxels, bandwidth of 956 Hz/pixel, repetition time of 15 ms, echo time of 1.23 ms and 2.46 ms, and flip angle 10 degrees were used. A 24-channel spine coil was used and parallel imaging using generalized auto calibrating partially parallel acquisition (GRAPPA) was applied. The μ-map image was created by the Dixon method (14, 15). This method obtains in-phase and reverse-phase images and adds or subtracts them to obtain images of water and fat. Scatter correction was done by the Relative-Single Scatter Simulation (SSS) method (16). PET images with MR-AC were compared to PET images with CT-AC (17).

PET/CT system

Data acquisition was done using a PET/CT system (Biograph mCT, Siemens Healthcare GmbH, Erlangen, Germany) with software versions VG51C. PET acquisition was done for 10 minutes in a list mode with a matrix size of 256×256 (voxel size 3.2×3.2×5.0). The CT imaging parameters were a tube voltage of 120 kV and an average tube current of 56 mA by auto-exposure. PET/CT images were reconstructed for only the signal part using CT-AC and Relative-SSS.

Data analysis

Positive and negative signals were evaluated with %-contrast calculated by the following formulae (18):

$$\%Q_{H,j} = \left(\frac{C_{H,j}/C_{B,j} - 1}{a_H/a_B - 1} \right) \times 100$$

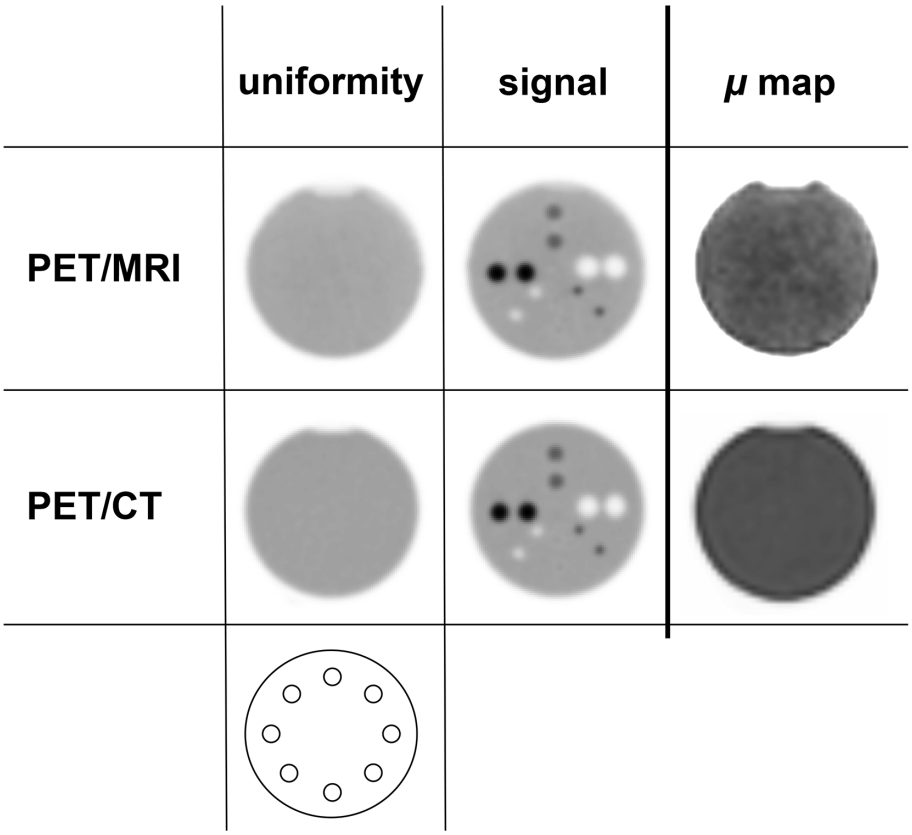

Figure 2 Images of the phantom acquired by PET/MRI and PET/CT. Image of the part without signal for uniformity and with signal part images are similar between PET/MRI and PET/CT on the basis of visual inspection. The image on the right is the μ-map images used for attenuation correction. The bottom schema shows the positions of eight ROIs on concentric circles of 15 mm in diameter for the BG slice without the signal.

$$\%Q_{C,j} = \left(1 - \frac{C_{C,j}}{C_{B,j}}\right) \times 100$$

$$\%N_j = \frac{SD_j}{C_{B,j}} \times 100$$

The PET/MRI and PET/CT data acquisition performed within 30 minutes in a row on the one day. PET images were analyzed by the dedicated workstation (Syngo Via, Siemens Healthcare GmbH, Erlangen, Germany). The size of the region of interest (ROI) was determined from the CT image. $C_{H,j}$ and $C_{C,j}$ are the average counts in the ROIs of the positive and the negative signals j, respectively, and $C_{B,j}$ is the average value of eight ROIs on concentric circles of 15 mm in diameter for the BG slice without the signal. aH is the radioactivity concentration in the positive signal, and aB is that in the background area. SDj is standard deviation within the ROI set in the background area for each sphere j. The %Nj is variation in image quality and the %-contrast is recognition of signal, which was compared with the calculated value of the PET/CT image.

Results

Figure 2 shows attenuation corrected PET images of PET/MRI and PET/CT. Both the uniformity images and signal images are presented. Attenuation of the glue was approximately 9.5 Hounsfield units (HU) on the CT image, which corresponded to a water segment by the Dixon method. The attenuation factor coefficient (cm^{-1}) of μ-map is 0 for air, 0.0224 for lung, 0.0854 for fat and bone marrow, and 0.1 for soft tissue and trabecular bone.

Soft tissue was used as the attenuation coefficient of μ-map in this study.

Table 1 summarizes the %-contrast of each positive and negative signal of 7 mm ϕ and 15 mm ϕ columns located at shallow and deep layer of the phantom. The %-contrasts of the positive shallow signals with PET/MR and PET/CT were 41.8% and 45.4%, respectively. And it of the positive deep signals with PET/MR and PET/CT were 40.7% and 44.9%. On the other hand, the %-contrasts of the negative shallow signals with PET/MR and PET/CT were 62.3% and 65.6%, respectively. And it of the negative deep signals with PET/MR and PET/CT were 60.7% and 63.7%. Moreover, the% Nj index of uniformity was 2.0% on PET/MRI images and 0.34%

Table 1 Comparison of %-contrast for PET/MRI and PET/CT measured by positive (A) and negative (B) signals of the hot and cold columns, respectively.

A

	7 mm ϕ columns		15 mm ϕ columns	
PET System	shallow	deep	shallow	deep
PET/MR	21.4	20.8	62.3	60.7
PET/CT	23.5	22.5	65.6	63.7

B

	7 mm ϕ columns		15 mm ϕ columns	
PET System	shallow	deep	shallow	deep
PET/MR	13.4	13.2	41.8	40.7
PET/CT	15.8	15.6	45.4	44.9

on PET/CT images. For negative signals that assume a decrease in myocardial blood flow, The image quality of MR-AC was almost the same as that of CT-AC. Consistency between the images after CT-AC and MR-AC correction were confirmed, and in particular, a stable MR-AC μ-map was obtained in the phantom study. Both were stable, but the PET/CT was slightly better. The positive and negative signals of the PET/MRI images seem almost the same as those of the PET/CT image, and the image quality is similar. The %-contrast was better for the PET/CT image than the PET/MRI image, and the positive signals were better than the negative signals. The deep signals showed several percent lower values for both positive and negative signals.

Discussion

We have constructed a prototype phantom for the performance test of PET/MRI, consists of two portions; signal part with two concentrations of hot columns filled with ^{18}F-FDG radioactive water and cold columns, and the other half portion uniformly filled with polyvinyl alcohol glue in the phantom. Reconstructed PET/MRI images are equivalent to PET/CT images. Quantitative evaluation of image quality has not been performed, because standardized procedure of performance test has not been specified.

In MRI performance test phantom, liquid paraffin (PH-31 41330-000, PH32 41330-030, Kyoto Kagaku, Kyoto, Japan) and polyvinyl alcohol (PVA) gel (90-401, Nikko Fines, Tokyo, Japan) are used in MRI performance test phantoms to ensure uniformity in high magnetic fields. However, these liquids are insoluble in water and it is difficult to mix ^{18}F radioactive water uniformly. In a phantom filled with ^{18}F radioactive water, the magnetic field does not reach deep due to the dielectric effect (13). If the inside of the phantom is water, it should be frozen for phantom study (19). Or other than water must be used (20). The performance evaluation phantom dedicated to MRI is a small phantom with a diameter of about 18 cm, and the phantom is filled with liquid paraffin or the like. And the size of a commercially available MRI performance test phantom is about 18 cm in diameter, and its size is the limit.

There have been reports by Esser PET (model PET/FL/P) (21) phantom and NEMA IQ phantom (22) so far. However, the following points are not clear in these reports. First, the relationship between FDG water and MR available solutions is unknown. Next, the uniformity of MR images has been significantly reduced or not shown. Moreover, the image processing method is not described in detail. Image reproducibility is difficult with the content of this report alone.

Besides these, the detectability of positive signals in the larger spheres that simulate ^{18}F-FDG accumulation in the tumor has been discussed in relation to the NEMA IEC Body Phantom Set™ (Model PET/IEC-BODY/P) (23). However, a basic evaluation procedure for the negative signal of the hypoperfusion site in ^{13}N-NH_3 myocardial perfusion PET has not been reported. Imaging of the negative signal (24), so-called decreased myocardial perfusion reserve (MPR) is important in the field of cardiac nuclear medicine (25). The Anthropomorphic Torso Phantom™ (Model ECT/TOR/P) is available as a myocardial phantom, but the time required for injecting the radioactivity accounts for increased radiation exposure to engaged workers.

Performance evaluation of PET is subject to the JIS T 61675-1:2016. This standard is subject to the international standard (23, 26). Evaluation of spatial registration of PET/MRI has been standardized (27), however, uniformity is not specified in JIS or NEMA. Under these circumstances, there is no commercially available phantom for the evaluation of PET/MRI images.

Therefore, in this study, we attempted to construct a simple phantom that can be used for the evaluation of PET/MRI system. We initially considered using oil (olive oil: Ajinomoto Co., Inc. Tokyo, Japan) instead of glue to be filled in the

phantom. The oil provides a stable μ-map with a CT of -120 HU, but it was extremely viscous and difficult to handle. Consequently, glue of lower viscosity was used to create the μ images. No significant difference was observed between the PET/MR image and the PET/CT image, and the negative signals are also well identified. But viscosity affects the uniformity of the μ-map in Figure 2. The present study indicated that our phantom was useful for image evaluation of PET/MRI system. Future development of a material that can be uniformly mixed with ^{18}F-FDG radioactive water is anticipated. As the reduction of patient radiation dose is always desirable, and MRI causes no radiation exposure, more widespread use of PET/MRI systems would be expected.

There are limitations that should be addressed in the present study. The suggested phantom is a prototype without performing sufficient examination, because performance evaluation for PET/MRI is not standardized at present. Therefore, images of the phantom are evaluated by the %-contrast. The purpose of the present study is not evaluating the performance of the phantom, but proposing a simple and easy-to-use phantom for possible image quality evaluation of PET/MRI.

Conclusion

The present study revealed that PET images with MR-AC using a μ-map created using a prototype phantom with glue as negative signal were the same as conventional PET images with CT-AC. This simple phantom would be used to validate performance of PET/MRI system.

Acknowledgments

The authors thank Ms Kaori Yamaki for technical assistance.

Sources of funding

A part of this work was supported by the Research Center for Radiation Disaster Medical Science and JSPS KAKENHI Grant Number JP22H03986.

Conflicts of interest

None.

Reprint requests and correspondence:
Yasuyuki Takahashi, PhD
Department of Radiation Science, Hirosaki University Graduate School of Health Sciences
66-1 Honcho, Hirosaki, Aomori 036-8564, Japan
E-mail: ytaka3@hirosaki-u.ac.jp

References

1. Masuda A, Yamaki T, Kunii H, Nemoto A, Kubo H, Tominaga H, et al. Inflammatory involvement in a patient with Leriche syndrome evaluated by ^{18}F-fluorodeoxyglucose PET/MRI. J Nucl Cardiol 2017; 24: 1819–21.
2. Roes SD, Kaandorp TAM, Marsan NA, Westenberg JJM, Dibbets-Schneider P, Stokkel MP, et al. Agreement and disagreement between contrast-enhanced magnetic resonance imaging and nuclear imaging for assessment of myocardial viability. Eur J Nucl Med Mol Imaging 2009; 36: 594–601.
3. Harper PV, Lathrop KA, Krizek H, Lembares N, Stark V, Hoffer PB: Clinical feasibility of myocardial imaging with $^{13}NH_3$. J Nucl Med 1972; 13: 278–80.
4. Rauch B, Helus F, Grunze M, Braunwell E, Mall G, Hasselbach W, et al. Kinetics of ^{13}N-ammonia uptake in myocardial single cells indicating potential limitations in its applicability as a marker of myocardial blood flow. Circulation 1985; 71: 387–93.
5. Muzik O, Beanlands RS, Hutchins GD, Mangner TJ, Nguyen N, Schwaiger M. Validation of nitrogen-13-ammonia tracer kinetic model for quantification of myocardial blood flow using PET. J Nucl Med 1993; 34: 83–91.
6. Carvajal-Juarez I, Monroy-Gonzalez A, Espinola-Zavaleta N, Meave-Gonzalez A, Alexanderson-Rosas E. PET/CT with ^{13}N-ammonia: characteristics and utility in coronary artery disease. Ann Nucl Cardiol 2019; 5: 63–8.
7. Mc Ardle B, Shukla T, Nichol G, deKemp RA, Bernick J, Guo A, et al. Long-term follow-up of outcomes with F-18-Fluorodeoxyglucose positron emission tomography imaging-assisted management of patients with severe left ventricular dysfunction secondary to coronary disease. Circ Cardiovasc Imaging 2016; 9: e004331.
8. Slart RHJA, Bax JJ, van Veldhuisen DJ, van der Wall EE, Dierckx RA, de Boer J, et al. Prediction of functional recovery after revascularization in patients with coronary artery disease and left ventricular dysfunction by gated FDG-PET. J Nucl Cardiol 2006; 13: 210–9.
9. Kim RJ, Fieno DS, Parrish TB, Harris K, Chen EL, Simonetti O, et al. Relationship of MRI delayed contrast enhancement to irreversible injury, infarct age, and contractile function. Circulation 1999; 100: 1992–2002.
10. Tadamura E, Yamamuro M, Kubo S, Kanao S, Saga T, Harada M, et al. Effectiveness of delayed enhanced MRI for identification of cardiac sarcoidosis: comparison with radionuclide imaging. AJR Am J Roentgenol 2005; 185: 110–5.
11. Kiko T, Yokokawa T, Misaka T, Matsuda A, Yoshihisa A, Yamaki T, et al. Myocardial viability with chronic total occlusion assessed by hybrid positron emission tomography/magnetic resonance imaging. J Nucl Cardiol 2021; 28: 2335–42.
12. National Electrical Manufactures Association. NEMA standards publication NU 2-2018. Performance measurements of positron emission tomographs (PETS). Rosslyn, VA, 2018.
13. Yang QX, Wang J, Zhang X, Collins CM, Smith MB, Liu H, et al. Analysis of wave behavior in lossy dielectric samples at high field. Magn Reson Med 2002; 47: 982–9.
14. Torrado-Carvajal A, Vera-Olmos J, Izquierdo-Garcia D, Catalano OA, Morales MA, Margolin J, et al. Dixon-VIBE

Deep Learning (DIVIDE) pseudo-CT synthesis for pelvis PET/MR attenuation correction. J Nucl Med 2019; 60 :429–35.
15. Shandiz MS, Rad HS, Ghafarian P, Karam MB, Akbarzadeh A, Ay MR. MR-guided attenuation map for prostate PET-MRI: an intensity and morphologic-based segmentation approach for generating a five-class attenuation map in pelvic region. Ann Nucl Med 2017; 31: 29–39.
16. Heußer T, Mann P, Rank CM, Schäfer M, Dimitrakopoulou-Strauss A, Schlemmer HP, et al. Investigation of the halo-artifact in ^{68}Ga-PSMA-11-PET/MRI. PLoS One 2017; 12: e0183329.
17. Kinahan PE, Townsend DW, Beyer T, Sashin D. Attenuation correction for a combined 3D PET/CT scanner. Med Phys 1998; 25: 2046–53.
18. Technology guideline for imaging of FDG-PET study. The Japanese Journal of Nuclear Medicine Technology 2007; 27: 425-456. [Article in Japanese]. http://jsnm.org/wp_jsnm/wp-content/themes/theme_jsnm/doc/FDG-PET_satsuzougijutsu GL.pdf.
19. Yoshida T, Urikura A, Hosokawa Y, Shirata K, Nakaya Y, Endo M. Apparent diffusion coefficient measurement using thin-slice diffusion-weighted magnetic resonance imaging: assessment of measurement errors and repeatability. Radiol Phys Technol 2021; 14: 203–9.
20. Sato E, Fukuzawa K, Takashima H, Yamatani Y, Takatsu Y, Hata J, et al. Evaluation of a polyethylene glycol phantom for measuring apparent diffusion coefficients using three 3.0 T MRI systems. Appl Magn Reson 2021; 52: 619–31.
21. Øen SK, Aasheim LB, Eikenes L, Karlberg AM. Image quality and detectability in Siemens Biograph PET/MRI and PET/CT systems-a phantom study. EJNMMI Phys 2019; 6: 16.
22. Ziegler S, Jakoby BW, Braun H, Paulus DH, Quick HH. NEMA image quality phantom measurements and attenuation correction in integrated PET/MR hybrid imaging. EJNMMI Phys 2015; 2: 18.
23. National Electrical Manufacturers Association: NEMA Standards Publication NU 2-2001, Performance Measurement of Positron Emission Tomographs. Rosslyn, VA, 2001.
24. Knešaurek K, Machac J. Comparison of ^{18}F SPECT with PET in myocardial imaging: a realistic thorax-cardiac phantom study. BMC Nucl Med 2006; 6: 5.
25. Tamaki N, Kusakabe K, Kumita S, Shimamoto K, Senda S, Nishimura T, et al. Guidelines for clinical use of cardiac nuclear medicine (JCS 2010). http: //jsnm. org/wp_jsnm/wp-content/themes/theme_jsnm/doc/shinzoukakuigakukensa_gl.pdf
26. Radionuclide imaging devices-Characteristics and test conditions-Part 1: Positron emission tomographs. IEC 61675-1:2013. 2.0.
27. Performance evaluation of positron emission tomographs. JESRA X-0073*E-2017. Japan Medical Imaging and Radiological Systems Industries Association, Tokyo, 2017.